Acta Materialia 139 (2017) 226–235

Contents lists available at ScienceDirect

Acta Materialia

journal homepage: www.elsevier.com/locate/actamat

Full length article

Classical-nucleation-theory analysis of priming in chalcogenide phase-change memory

Jiri Orava [a, b, *], A. Lindsay Greer [a, b, **]

[a] Department of Materials Science & Metallurgy, University of Cambridge, 27 Charles Babbage Road, Cambridge CB3 0FS, United Kingdom
[b] WPI Advanced Institute for Materials Research, Tohoku University, 2-1-1 Katahira, Aoba-ku, Sendai 980-8577, Japan

ARTICLE INFO

Article history:
Received 17 May 2017
Received in revised form
24 July 2017
Accepted 7 August 2017
Available online 8 August 2017

Keywords:
Amorphous materials
Classical nucleation theory
Phase-change chalcogenides
Phase transformation kinetics
Rapid solidification

ABSTRACT

The chalcogenide $Ge_2Sb_2Te_5$ (GST) is of interest for use in phase-change memory. Crystallization is the rate-limiting step for memory operation, and can be accelerated by the prior application of a "priming" heating pulse. There is characteristic fading of the priming effect if there is a time interval between the priming pulse and the main heating pulse to achieve crystallization. We apply classical nucleation theory to interpret these effects, based on a fitting of nucleation kinetics (steady-state and transient) over the full temperature range of the supercooled liquid. The input data come from both physical experiments and atomistic simulations. Prior studies of conventional glass-formers such as lithium disilicate preclude any possibility of fading; the present study shows, however, that fading can be expected with the particular thermodynamic parameters relevant for GST and, possibly, other phase-change chalcogenides. We also use the nucleation analysis to highlight the distinction between GST and the other archetypical chalcogenide system (Ag,In)-doped Sb_2Te. Classical nucleation theory appears to be applicable to phase-change chalcogenides, and to predict performance consistent with that of actual memory cells. Nucleation modeling may therefore be useful in optimizing materials selection and performance in device applications.

1. Introduction

Chalcogenide phase-change (PC) materials, exemplified by $Ge_2Sb_2Te_5$ (GST) and (Ag,In)-doped Sb_2Te (AIST), have been widely studied for their use in optical (DVD, Blu-ray™) and electrical (phase-change random-access memory, PC-RAM) data recording [1]. These applications exploit the high contrast in reflectance and resistance upon reversible glass-to-crystal transitions. Recent interest has included such applications as display and data visualization [2], and synaptic switching [3]. In the case of PC-RAM, a relatively low-power electrical pulse heats the glassy chalcogenide above its glass-transition temperature, T_g, crystallizing it (SET operation). The reverse switching is achieved by heating the crystal with a relatively short high-power pulse above its melting temperature, T_m, and subsequent rapid quenching (at 10^9–10^{11} K s^{-1} [4,5]) of the liquid into the glassy state (RESET operation).

Crystallization is of particular interest as the SET operation is the rate-limiting step for memory switching. At and just below their melting temperatures, the PC chalcogenide liquids have low viscosities [6–11], similar to those of liquid pure metals [12]; the consequent high molecular mobility allows the SET times to be short (of order 1–10 ns). Even so, for PC-RAM in particular, there are ongoing efforts to shorten the crystallization time and also to reduce the energy needed to switch between memory states.

Early kinetics studies showed that differences in the crystallization rates of glassy GST samples are largely due to differences in the kinetics of crystal nucleation [13]. In isothermal annealing, there is an incubation time before the onset of crystallization, and this time is temperature-dependent [13]. In GST, the incubation time is much shorter in melt-quenched than in as-deposited amorphous films, and this was attributed to a population of quenched-in crystallites [13,14]. The generation of such crystallites is a *priming* effect [15]. Priming is of interest in several contexts [16–18], but the present interest in priming of phase-change memory (PCM) has been driven by the work of Loke et al. [19], who showed that applying a constant low voltage ahead of the SET pulse (Fig. 1) could reduce the crystallization time from 5 ns to 0.5 ns This dramatic acceleration was attributed to 'pre-structural

* Corresponding author. University of Cambridge, United Kingdom.
** Corresponding author. University of Cambridge, United Kingdom.
E-mail addresses: jo316@cam.ac.uk, orava.jiri@gmail.com (J. Orava), alg13@cam.ac.uk (A.L. Greer).

http://dx.doi.org/10.1016/j.actamat.2017.08.013

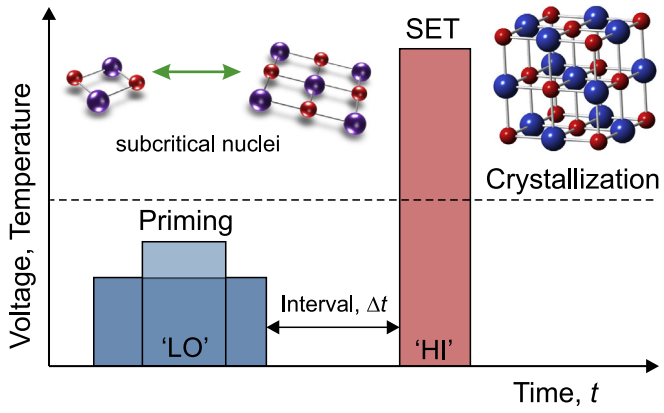

Fig. 1. In the operation of PC-RAM, a high-power (HI) 'SET' electrical pulse is used to heat an amorphous chalcogenide causing it to crystallize. The application of a prior low-power (LO) *priming* pulse can reduce the total time and energy involved in crystallization [18,19]. In priming, a variety of combinations of pulse length and power have been used, with or without the interval Δt. The atomic configurations illustrate schematically that priming works by generating subcritical crystalline clusters that aid the nucleation of the ultimate crystalline structure. (For interpretation of the references to colour in this figure legend, the reader is referred to the web version of this article.)

ordering', interpreted as a growth in the population of subcritical crystalline nuclei (clusters) in the amorphous phase.

In an idealized glass devoid of subcritical crystalline clusters, annealing at a given temperature leads to a cluster size distribution with populations increasing with time until they reach a steady-state distribution characteristic of the anneal temperature. The evolution of the cluster size distribution in glasses was first modeled in detail by Kelton et al. [20] to understand the origin of the incubation time in the context of classical nucleation theory (CNT). Their rate-equation analysis showed that a pre-existing distribution of clusters can shorten the effective time-lag for nucleation. Focusing first on thermodynamic and kinetic parameters typical for an oxide glass (lithium disilicate, LS_2) and later on metallic glasses, Kelton and Greer showed that numerical modeling of transient size distributions could be useful in understanding glass-forming ability and in validating the kinetic model in CNT [21–23].

Modeling of this type was first extended to a chalcogenide (GST) by Senkader and Wright [24], who used it successfully to fit the incubation time results mentioned above [13]. They noted that the crystallization of a PCM cell takes place entirely in a transient nucleation regime [24].

For PC chalcogenides (in contrast to the lack of work on other amorphous systems) there have been several microscopical studies of cluster distributions. These have been based on fluctuation transmission electron microscopy (FTEM), permitting statistical detection of nanoscale ordering, attributable to subcritical clusters. While the absolute size distribution cannot be precisely determined, relative changes can be reliably inferred [25]. Comparing cluster size distributions in GST and AIST in various states, it is found that:

- subcritical size distributions can be detected and can be altered by annealing, laser treatment or melt-quenching [26];
- pre-existing larger (smaller) cluster populations are associated with shorter (longer) nucleation incubation times [25–27];
- annealing effects (larger population, shorter incubation) saturate when the steady-state cluster size distribution is established [25];
- in GST melt-quenching gives more and larger clusters than in the as-deposited state, and this effect is greater on slower quenching [28];
- in AIST melt-quenching gives fewer and smaller clusters [27];
- the characteristic behaviors of GST and AIST are readily distinguished [27];
- N-doping effects in GST can be interpreted in terms of nucleation kinetics [29].

These microscopical observations are complemented (i) by kinetic (rate-equation) studies [24,30] and (ii) by atomistic simulations of ordering and the onset of crystallization in liquid chalcogenides [19,31–35]. Together, these studies provide support for interpretations of phase-change kinetics based on classical models of crystal nucleation and growth. These studies have focused on crystallization kinetics within the volume of the amorphous chalcogenide. Given the small volume of PCM cells, there has to be concern about surface and interface effects, particularly on crystal nucleation. Nevertheless, many studies suggest that there is a wide range of conditions under which surface and interface effects can be ignored [13], especially in the absence of oxidation [36].

We use CNT to examine the evolution of crystalline cluster size distributions, especially to explain priming effects in GST. There are many reasons for interest in multiple-pulse interactions, including the parallel writing of memory arrays [18] and the possibility of undesirable *read-disturb* [37], but our immediate focus is on improving SET switching. Lee et al. showed that the use of prior priming pulses can reduce not only the duration of the SET pulse necessary for switching (as shown earlier [19]), but also the total pulse duration and the total energy. That is: the total duration of the priming and shortened SET pulses is shorter (by up to 33%) than the duration of the SET pulse that would be necessary without priming, and similarly for the total energy (up to 43% less) [18].

Classical analyses of crystallization kinetics show that the rates of both nucleation and growth show a maximum as a function of temperature between T_g and T_m, and that the maximum in nucleation rate occurs at significantly lower temperature than that for growth. These maxima are exploited in two-stage heat treatments to control the microstructural development in devitrification of oxide glasses, the first, lower-temperature treatment being used to obtain the desired population of nuclei, and the second, higher-temperature treatment being used to grow crystallites to the desired size. As noted in several works [18,19,34], the priming treatment and the SET pulse applied to PC chalcogenides can be considered analogous to these two stages, and, if so, priming should be best achieved in the temperature range of the maximum in nucleation rate.

If there is an interval Δt in which no current is applied, between the priming pulse and the SET pulse (Fig. 1), the effect of the priming pulse fades (substantially, but not totally), with a relaxation time of ~1 μs [18]. Lee et al. considered possible electrical and thermal effects to explain why the required SET pulse length increases with increasing Δt after the priming pulse, but they concluded that the *fading* must be intrinsic to the chalcogenide material (Ref. [18], Suppl. Info.). In general, it is considered that priming and switching effects in PCM are purely thermal, arising from Joule heating [38].

As shown schematically [18], during the priming pulse a subcritical cluster size distribution develops and increases towards the steady-state distribution for the temperature established during the pulse. At the end of the priming pulse, the temperature drops, and the cluster size distribution, if it changes at all, must evolve towards the steady-state distribution characteristic of a

lower temperature. But would such an evolution be to lower populations (as required to explain the fading), or to higher populations? Our existing understanding is from the extensive quantitative modeling of crystallization in oxide glasses. Fig. 2a shows two steady-state cluster size distributions in the supercooled liquid of LS_2 [20,39,40]; in the region of the cluster size relevant for subsequent annealing to grow the crystals, the higher steady-state populations are clearly associated with the lower temperature. From this we would expect that any evolution of the subcritical crystal cluster size distribution after priming would enhance rather than diminish the priming effect. The observed fading of the priming effect in chalcogenides is thus opposite to what would be expected from the existing studies of a system such as LS_2.

The present work addresses this issue, and shows that the observed fading effects, far from contradicting CNT, actually support its applicability in analyzing SET kinetics in PCM. We analyze GST in detail, but also contrast with the nucleation behavior in AIST.

2. Classical nucleation theory

We adopt the nomenclature and formalism of Kelton et al. [20,40] in describing a system in which freezing is congruent, and the crystal nucleation in the supercooled liquid (i.e. in the system above its T_g) is taken to be homogeneous. Crystalline clusters, assumed spherical, are characterized by their size, expressed as the number, n, of atoms for GST and AIST in this study (and formula units for LS_2 [20]) that they contain. We take the reversible work of formation of a cluster to be:

$$W(n,T) = n\Delta\mu + (36\pi)^{1/3}\nu^{2/3}n^{2/3}\sigma, \quad (1)$$

where $\Delta\mu$ is the change in free energy per atom (or formula unit) on crystallization, ν is the atomic volume, and σ is the energy per unit area of the interface between the crystal and the supercooled liquid. The first term on the right-hand side of Eq. (1) is negative, and the second term positive. The work shows a maximum at the critical size n^* given by:

$$n^*(T) = \frac{32\pi\nu^2\sigma^3}{3|\Delta\mu|^3}. \quad (2)$$

Nucleation is considered to occur when clusters first exceed this critical size. The magnitude of $\Delta\mu$ increases roughly linearly with the supercooling ΔT below the congruent melting temperature T_m, while in contrast ν and σ are only weakly dependent on T; consequently n^* decreases as T is lowered, roughly in proportion to ΔT^{-3}. The equilibrium population of clusters, $N^{eq}(n,T)$, i.e. their size distribution, per mole of material, is given by:

$$N^{eq}(n,T) = N_A \exp\left(-\frac{W}{k_B T}\right), \quad (3)$$

where N_A is Avogadro's number and k_B is Boltzmann's constant. At a given temperature, $N^{eq}(n)$ shows a minimum at n^* (Fig. 2b). Because the post-critical ($n > n^*$) clusters are in effect consumed by their growth into macroscopic crystals, the distribution $N^{eq}(n)$ cannot be established; instead the cluster sizes in an isothermally annealed glass tend to a steady-state distribution with lower populations (strictly, this is a quasi-steady-state distribution, because the population of atoms not in clusters, i.e. *monomers* in the terminology of CNT, is depleted over time) [20,40]. This distribution $N^{st}(n)$ tends to $N^{eq}(n)$ as n tends to one, and $N^{st}(n^*) = \frac{1}{2}N^{eq}(n^*)$ (Fig. 2b). In this distribution there is a forward

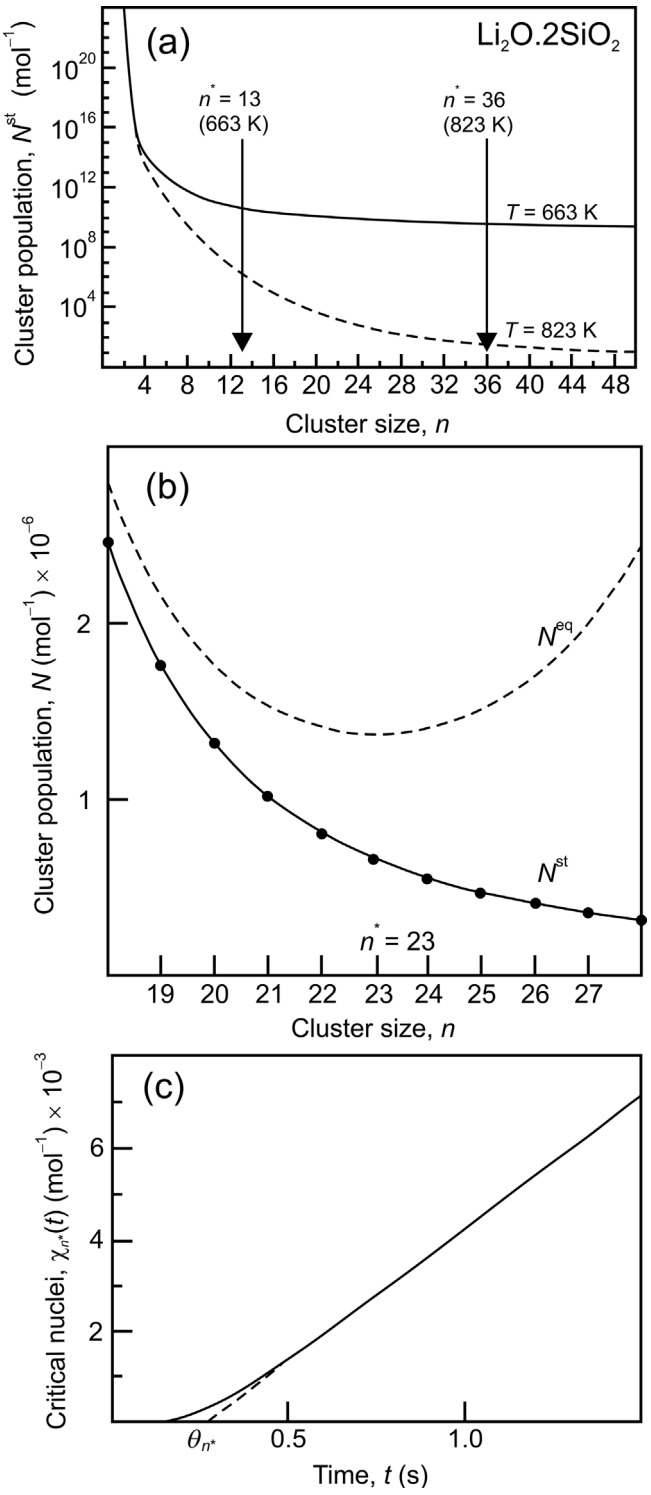

Fig. 2. Calculations of the populations of crystalline clusters (n formula units) in the supercooled liquid of lithium disilicate (LS_2, T_g = 728 K). (a) Steady-state size distributions and critical sizes at 663 K and 823 K. (b) size distributions in the region of the critical size ($n^* = 23$) at 750 K. The steady-state population $N^{st}(n)$ (dots obtained by numerical simulation) is compared with the equilibrium population $N^{eq}(n)$. (c) The number of critical nuclei $\chi_{n^*}(t)$ formed as a function of anneal time at 820 K. It is assumed that there are no clusters pre-existing before the anneal. The effective time-lag θ_{n^*} is marked. Redrawn and modified from (a) Ref. [39,40], (b,c) Ref. [20], with permission. (For interpretation of the references to colour in this figure legend, the reader is referred to the web version of this article.)

flux from clusters of size n to size $(n+1)$, and a backward flux between the same two sizes. The forward flux exceeds the backward by an amount, independent of n, that is the steady-state nucleation rate I^{st} given, per mole, by:

$$I^{st}(T) = \gamma\left(\frac{\sigma}{k_B T}\right)^{1/2} \nu^{1/3} 4\left(\frac{8}{81\pi^2}\right)^{1/6} N^{eq}(n^*), \quad (4)$$

where γ is the temperature-dependent molecular jump frequency. This frequency is related to the diffusivity D [20] and, through the Stokes–Einstein relation [41], to the viscosity η:

$$\gamma(T) = \frac{6D}{\lambda^2} = \frac{2k_B T}{\pi\lambda^3\eta}, \quad (5)$$

where λ is an effective molecular diameter (or jump distance), for GST taken to be 0.3 nm [7,9].

The analysis of experimental results must relate to steady-state cluster size distributions, but there is no simple analytical form for these. Instead we calculate (using Eq. (3)) equilibrium distributions up to the critical size (but not beyond, where the upturn, see Fig. 2b, in $N^{eq}(n)$ is unphysical). $N^{st}(n)$ is closely approximated by $N^{eq}(n)$, to which homogeneous nucleation frequencies are directly proportional.

It takes time at any annealing temperature to establish the steady-state size distribution of crystalline clusters. Most studies have focused on the idealized case in which there are no pre-existing clusters at the start of an isothermal anneal. Only as some clusters reach the critical size does nucleation formally begin, and ultimately a constant (steady-state) nucleation rate is established. The total number of nuclei generated at the critical size n^* as a function of time t, denoted as $\chi_{n^*}(t)$, takes the form shown in Fig. 2c: ultimately $\chi_{n^*}(t)$ is linearly related to time, but with an *effective time-lag* θ_{n^*} relative to the start of the anneal. This time-lag (closely related to other measures such as the *incubation time* or *transient time*) is temperature-dependent and to a reasonable approximation is given [20] by:

$$\theta_{n^*}(T) = k_B T\left(\frac{32\pi\nu^2}{3}\right)^{1/3} \frac{\sigma}{\gamma|\Delta\mu|^2}. \quad (6)$$

As critical nuclei are too small to be detected, there is no direct access to their population as they are produced. The nucleated crystals take some time to become detectable (to reach observable size), and correspondingly the effective time-lag for their appearance is longer than θ_{n^*}. Practically measurable time-lags are typically no more than one order of magnitude longer than θ_{n^*} [20], though the relationship can be complex [42].

3. Fitting crystal nucleation kinetics in GST

We now analyze the crystal nucleation kinetics in GST, to obtain a self-consistent fitting of experimental and atomistic-simulation results. We aim for a quantitative description similarly effective to that achieved for LS_2 [23]. There are three key variables, each dependent on temperature.

The first is the *mobility*, characterized by the molecular jump frequency γ. For LS_2, $\eta(T)$ has been directly measured, and Eq. (5) was used to obtain $\gamma(T)$. The validity of Eq. (5) has been assessed [41] for several supercooled liquids showing a wide range of *fragility*, (characterizing the form of $\eta(T)$, and quantified as $m = \left[\mathrm{d}\log_{10}\eta/\mathrm{d}(T_g/T)\right]_{T=T_g}$ [43]): the Stokes–Einstein relation is obeyed closely for a liquid of low m such as LS_2 ($m \approx 22$) [41,44]. For GST, the mobility has been best characterized in relation to the crystal growth rate $U(T)$, and was first determined indirectly through ultra-fast differential scanning calorimetry [7]. Fitting over the entire supercooled liquid region, it is found that the maximum growth rate $U_{max} \approx 1$ m s^{-1} at ~$0.76T_m$. The form of $U(T)$ has been broadly confirmed by subsequent studies [30,44–46] using a wide variety of techniques [47]. Fitting of the thermodynamic driving force for crystallization (see below) allows the kinetic coefficient for crystal growth $U_{kin} = D/\lambda$ to be extracted from $U(T)$. At T_g, the viscosity is conventionally set at 10^{12} Pa s, yet a simple application of the Stokes–Einstein relation to $U_{kin}(T)$ gave a viscosity at T_g of only ~10^7 Pa s [7]; in essence, the extrapolated crystal growth rate near T_g is faster than would be expected from the viscosity. This discrepancy could be explained as a progressive decoupling of crystal growth from viscous flow as the temperature is lowered from T_m to T_g, such that $U_{kin} \propto \eta^{-0.67}$. This decoupling would be expected [41] for a liquid of high fragility such as GST ($m \approx 90$ [44]). In the present work, we adopt an existing description of $\eta(T)$ [7], and we consider whether or not there is some decoupling of $U_{kin}(T)$, and therefore of $\gamma(T)$, from $\eta(T)$. With mechanical constraint, varying degrees of decoupling may be possible [48].

The second variable is the thermodynamic *driving force* for crystallization $\Delta\mu$. For LS_2, this has been directly measured and, to a good approximation, its magnitude increases linearly with supercooling below the congruent melting point of $T_m = 1300$ K [23]; this linear dependence is known as the *Turnbull approximation*. For GST, in contrast, we adopt the expression for $\Delta\mu(T)$ due to Thompson and Spaepen [49]:

$$\Delta\mu = \left[\frac{\Delta H_m \Delta T}{T_m}\left(\frac{2T}{T_m + T}\right)\right]\frac{1}{N_A}, \quad (7)$$

where ΔH_m is the latent heat of melting per mole (Table 1). Equation (7) provides a reasonable description for chalcogenide systems [4,50] and, in any case, is necessary to ensure consistency with the analysis from which $U_{kin}(T)$ was derived [7]. According to Eq. (7), the free-energy change driving crystallization increases rather less with supercooling than would be expected from a linear extrapolation of the behavior near T_m [4].

The third variable is the *interfacial energy*, σ per unit area, between the glass/liquid and crystal phases. As σ is not readily measurable, for both LS_2 and GST it has been treated as an adjustable parameter. For LS_2 it was possible to fit σ as a function of temperature, upon which it has a weak linear dependence [23]; for GST, with greater uncertainty in mobility and in driving force, we

Table 1
Thermodynamic and kinetic parameters for the glass-forming systems: $Li_2O.2SiO_2$ (lithium disilicate, LS_2), $Ge_2Sb_2Te_5$ (GST) and (Ag,In)-doped Sb_2Te (AIST).

	$Li_2O.2SiO_2$	GST	AIST
T_m (K)	1300 [21]	900 [24]	810 [54]
T_g (K)	728 [21,23,44]	383 [7]	378 [9,11]
T_{rg}	0.56	0.42(6)	0.46(7)
ΔH_m (kJ mol^{-1})	52 [21]	12.13 [24]	16.1 [54]
ν (m^3)	9.96×10^{-29}	3.06×10^{-29}	3.08×10^{-29}
σ (J m^{-2})	0.15 [21]	0.075	0.11[a]
$\gamma(T)$ (s^{-1})	$0.094 + (7 \times 10^{-5})T$ [23] Refs. [23,53]	$\eta(T)$, $U_{kin}(T)$ [7]	$\eta(T)$ [9]

T_m – melting point; T_g – glass-transition temperature; T_{rg} – reduced glass-transition temperature ($= T_g/T_m$); ΔH_m – latent heat of melting per mole; ν – monomer volume (i.e. per atom for GST and AIST, and per formula unit for LS_2); σ – crystal-liquid interfacial energy; $\gamma(T)$ – temperature-dependent atomic jump frequency (details of the temperature-dependent mobility used to calculate $\gamma(T)$ using the Stokes–Einstein relation are given in the references).

[a] Kalb et al. [54] showed that σ of AIST is greater than for GST, consistent with the relative values of their enthalpies of melting [39].

can reasonably only make a fitting with σ as a temperature-independent constant. In any case, for many glass-forming systems σ changes by less than 10% over a wide temperature range [51].

As noted in earlier work [20,23] on deriving nucleation parameters, it is valuable to have data on both steady-state nucleation rates and nucleation time-lags. While the nucleation rates are very strongly dependent on σ, the time-lags are not (being simply proportional to σ). In contrast to LS_2, very few nucleation-rate and time-lag data are available for GST, but fortunately enough to achieve a preliminary fitting, especially when data from atomistic simulations are included.

To obtain the time-lag using Eq. (6), we need a value for σ. We use the expression of Spaepen and Meyer [52]:

$$\sigma = \frac{\Delta H_m \alpha_m}{(N_A V^2)^{1/3}} \frac{T}{T_m}, \tag{8}$$

where $\alpha_m$is a geometric constant taken to be 0.86 (the value for the interface between a liquid and a cubic close-packed crystal) and V is the molar volume. With parameters as in Table 1, and taking T to be the glass-transition temperature T_g, Eq. (8) gives $\sigma = 0.075$ J m^{-2}. We obtain $\gamma(T)$ from crystallization kinetics measured [7], making two alternative assumptions: (i) that $\gamma(T)$ is simply related to the viscosity $\eta(T)$ by the Stokes–Einstein relation (Eq. (5)), and (ii) that $\gamma(T)$ scales with $U_{kin}(T)$, somewhat decoupled from $\eta(T)$ as discussed above. The values of $\gamma(T)$ in the two cases match at T_m.

Fig. 3a shows the predicted form of $\theta_{n^*}(T)$ for these two cases, allowing comparison with values of the nucleation time-lag in GST given in the literature. From molecular-dynamics simulations [19,55,56] values of the time-lag are available at 600 K and 700 K. As these simulations show the earliest stages of crystal formation, the time-lags obtained can be considered to be those at the critical size, i.e. θ_{n^*} as given by Eq. (6). Nucleation time-lags have also been measured in physical experiments on isothermally annealed samples, from the first detection of crystallization: in transmission electron microscopy (TEM) [57], in reflectometry [13], or in resistometry [58]. The time-lag can also be derived just as is shown in Fig. 2c from TEM data on $\chi(t)$ [59,60]. All of these time-lags, which must be somewhat longer than the fundamental θ_{n^*}, have been measured near to T_g in the range 390–420 K, and are also shown on Fig. 3a. The temperature dependence of the measured time-lag is clearly weaker than the predicted variation of θ_{n^*}. There are difficulties in interpreting effective activation energies in this region near T_g, including uncertainty over the value of T_g itself (Ref. [7], Suppl. Info.).

Considering the measured limits of the time-lag, it is clear that taking $\gamma(T)$ directly from $\eta(T)$ via the Stokes–Einstein relation gives a reasonable fit, without any adjustment. If, instead, $\gamma(T)$ is taken from $U_{kin}(T)$, the calculated values of θ_{n^*} do not span a wide enough range to match the measured values. We conclude that, for the processes involved in forming a crystalline nucleus (apparently in contrast to those involved in its growth), there is little or no evidence for decoupling from the viscosity. The extent of decoupling in nucleation merits further study, for example through atomistic simulation.

Assuming a mobility obtained directly from the Stokes–Einstein equation (i.e. without decoupling), we proceed to adjust the value of σ to match the available data on nucleation rates. (The weak dependence of θ_{n^*} on σ means that there is no need to revisit the fitting of $\gamma(T)$ discussed above.) Unfortunately, as reviewed by Kalb et al. [61], direct observations of nucleation rates in GST are very rare. Furthermore, such observations in TEM samples are subject to effects from the surfaces of the thin foil and from the electron beam. We nevertheless take the values determined by Privitera et al. [59] close to T_g (in the range 403 K–416 K) and assume that these represent homogeneous nucleation rates. The rate calculated using the estimated value of $\sigma = 0.075$ J m^{-2} (Eq. (8) and Table 1) agrees well with the measurements by Privitera et al. [59]. Using Eq. (4), and adjusting the value of σ (which has its main effect

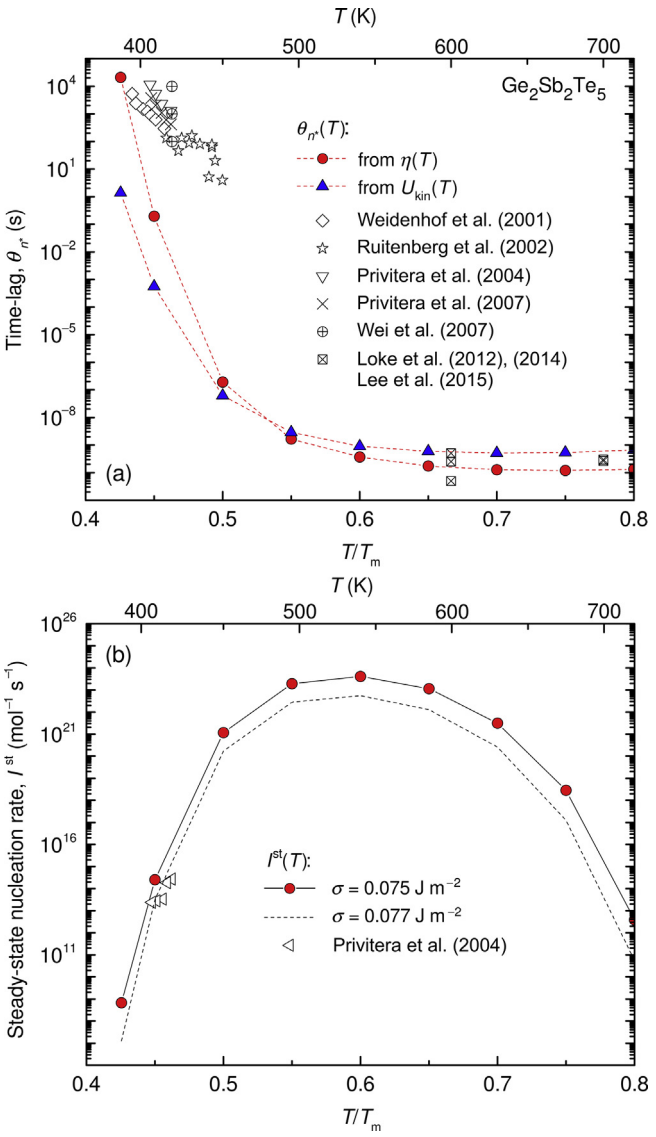

Fig. 3. Congruent crystallization in supercooled liquid $Ge_2Sb_2Te_5$ (GST): (a) the nucleation time-lag θ_{n^*}, and (b) the steady-state homogeneous nucleation rate I^{st}, as a function of the homologous temperature. To calculate $\theta_{n^*}(T)$, the atomic jump frequency $\gamma(T)$ is derived from the viscosity $\eta(T)$, or from the kinetic coefficient for crystal growth $U_{kin}(T)$ [7]; the derivation from $\eta(T)$ provides a better fit to time-lags measured in physical experiments just above the glass-transition temperature ($T_g = 383$ K) [13,57–60]; both mobilities merge at $T/T_m > 0.5$, providing a good fit to ab-initio molecular-dynamics (MD) simulations (squares with crosses) at 600 K ($0.67T_m$) and 700 K ($0.78T_m$) [18,19,56]. Using $\gamma(T)$ derived from $\eta(T)$, $I^{st}(T)$ is calculated for $\sigma = 0.075$ J m^{-2} (Table 1); fitting the $I^{st}(T)$ (the black solid line) to measured data (open triangles [59]) gives the crystal-liquid interfacial energy $\sigma = 0.077$ J m^{-2}. Details: Weidenhof et al. [13] – as-prepared single film GST, thickness $d = 85$ nm, optical reflectometry; Ruitenberg et al. [57] – as-prepared GST, $d = 25$ nm, sandwiched between Si_3N_4 layers (d ~2 nm), in-situ TEM; Privitera et al. [59,60] – chemically-etched GST, original $d = 50$ nm, in-situ TEM; Wei et al. [58] – as-prepared GST, $d = 3.5$, 10 and 100 nm, sandwiched between $ZnS:SiO_2$ (d ~50 nm) measured by electrical resistometry; Loke et al. [19] and Lee et al. [55,56] – ab-initio molecular-dynamics simulations, 180 atoms. (For interpretation of the references to colour in this figure legend, the reader is referred to the web version of this article.)

through its influence on $N^{eq}(n^*)$) it is possible to fit these values as shown in Fig. 3b. This fitting gives $\sigma \approx 0.077$ J m^{-2}, and we conclude, considering the possible errors in $I^{st}(T)$ measurements, that the value already obtained from Eq. (8), $\sigma = 0.075$ J m^{-2} is a sufficiently good estimate.

We compare this value of σ with other estimates in the literature. Values quoted for PC materials are in the range 0.03 to 0.1 J m^{-2} [24,62–65]. Liquid GST can be supercooled by up to 42.5 K under a B_2O_3 flux; as the nucleation in this case may be heterogeneous, the derived value of $\sigma = 0.04$ J m^{-2} must be regarded as a lower-bound estimate [4]. In fitting the predictions of a nucleation simulator to observed polycrystalline grain size distributions, Burr et al. derived $\sigma = 0.06$ J m^{-2} [30]. The interfacial energy can also be estimated from the size of a critical nucleus, and this size may be suggested by molecular-dynamics simulations. Lee and Elliott [55] found that for GST at 600 K, the probabilities of cluster growth or shrinkage are roughly equal for clusters composed of 5–10 connected cubes, i.e. with 22–33 atoms in total. The radius of a sphere with volume matching that of 8 cubes (i.e. $2 \times 2 \times 2$ as in the inset at upper right of Fig. 1) is 0.56 nm. Taking this as the critical radius r^*, calculating $\Delta\mu$ from Eq. (7), and noting that $r^* = 2\sigma v/\Delta\mu$, we obtain $\sigma = 0.05$ J m^{-2} (the value of 5 mJ m^{-2} in Ref. [55] appears to be in error). As Lee and Elliott note, the critical clusters may be somewhat larger if they are deemed to include some quasiordered regions, and correspondingly the estimate of σ would then be higher. We conclude that the value of $\sigma = 0.075$ J m^{-2} obtained in the present work is consistent with other studies [24,30,62–65].

The most comprehensive previous attempts [24,30] to fit crystal nucleation kinetics in GST have used the rate-equation approach of Kelton et al. [20]. Senkader and Wright fitted behavior only near to T_g over a narrow temperature range in which it was adequate to take $\gamma(T)$ to have an Arrhenius temperature dependence [24]. They did not adjust σ, but took it to be 0.1 J m^{-2}. The nucleation simulator developed by Burr et al. [30], mentioned above, was used to model the development of the polycrystalline microstructure in TEM membranes as they are continuously heated at different rates. This approach is particularly thorough, but fits the kinetics only in the narrow temperature range, 411–425 K, in which the crystallization occurs. The maximum heating rate, 6.3 K s^{-1}, is far below the range relevant for device operation, highlighting the interest in extrapolating to higher-temperature behavior. According to the value of T_g (428 K) assumed by these authors, the crystallization takes place in the glass and the fitting is to the type of temperature dependence appropriate for the glass and not the supercooled liquid. Thus the potential for extrapolation to higher temperatures is limited, and we cannot use their data as input for our fitting. Burr et al. do, however, suggest a form of $I^{st}(T)$ in the supercooled-liquid range that is broadly similar to that in Fig. 3b.

Unlike these previous analyses, we have included consideration of atomistic-simulation data. By so doing, we can attempt a fitting of nucleation kinetics over the entire temperature range of the supercooled liquid. Conceptually, this is similar to the approach taken to fitting the nucleation kinetics in LS_2 [23], although GST is a very different case. In LS_2, the kinetics of crystal nucleation and growth are sufficiently sluggish that crystallization can be interrupted at any stage by terminating the anneal. It follows that nucleation and growth rates can be determined directly from crystallite populations and sizes observed in quenched-in microstructures; furthermore, the microstructural scale is mostly observable optically. In contrast, in GST the maximum nucleation rate I_{max} is ~15 orders of magnitude higher, and the maximum growth rate U_{max} is ~5 orders higher [44], than in LS_2. Correspondingly the microstructure, which scales as $(U/I)^{1/4}$, is 2–3 orders of magnitude finer than in LS_2, resolvable only in TEM.

4. Cluster size distributions in LS_2 and GST

For LS_2, we build on previous quantitative modeling of crystal nucleation in the supercooled liquid [23], discussed briefly above and with key parameters as listed in Table 1. As noted in Section 2, we use equilibrium cluster-size distributions as readily calculated (Eq. (3)) close approximations to the steady-state distributions. Fig. 4a shows $N^{eq}(n)$ at selected values of homologous (or reduced) temperature T_r ($= T/T_m$). The distributions are consistent with those underlying earlier work [23], but have been calculated for a much wider range of T_r. The present work is concerned only with the comparatively rapid kinetics in the supercooled liquid ($T > T_g$). For LS_2 the reduced glass-transition temperature T_{rg} ($= T_g/T_m$) is 0.56, and the size distributions for lower values of T are unphysical

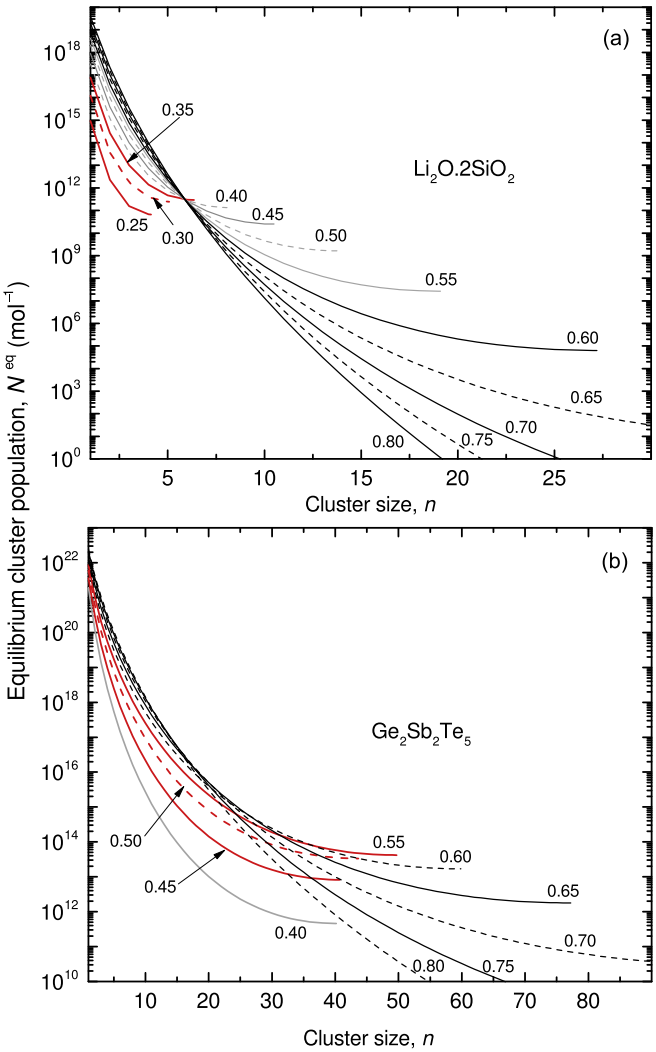

Fig. 4. Equilibrium subcritical cluster size distributions for crystallites in (a) LS_2 and (b) GST. The curves are labeled with the homologous temperature (T/T_m) and end (if within the range of the figure) at the critical size n^*. Curves colored gray, rather than black, are for temperatures below the glass transition ($T_g/T_m = 0.56$ for LS_2, and 0.43 for GST) and show distributions that are considered physically inaccessible; those colored red indicate the regime in which lower temperature is associated with lower cluster populations. This regime is not physically accessible for lithium disilicate, but for GST is relevant to explain the observed fading (with increasing interval Δt, Fig. 1) of the effect of priming pulses. (For interpretation of the references to colour in this figure legend, the reader is referred to the web version of this article.)

(shown in gray in Fig. 4a). For cluster sizes less than six, populations decrease with decreasing T_r, but for $T_r > 0.56$, the changes are negligible. Otherwise, within the entire physically accessible range, we can conclude that equilibrium (and, by extension, steady-state) cluster size distributions have higher populations at lower temperatures. This has already been seen in Fig. 2a and, as noted in Section 1, is inconsistent with fading effects of the type seen in the PCM priming experiments of Lee et al. [18].

Fig. 4b shows equilibrium cluster size distributions, not previously estimated, for GST, for which $T_{rg} = 0.43$. As in Fig. 4a, the endpoints of the curves, when visible, correspond to n^*. For $T_r \geq 0.55$, the equilibrium cluster populations are higher at lower temperature, the same trend as is shown in LS_2. In contrast, however, from T_{rg} up to $T_r = 0.55$, there is a physically accessible regime, not evident for LS_2, in which cluster populations can fall by as much as an order of magnitude as the temperature is decreased (but still in the supercooled liquid). This opens up the possibility of fading of the priming effect as Δt increases (Fig. 1). The subcritical cluster size distributions seen in the work of Burr et al. (top-left inset in Fig. 6 in Ref. [30]) may show this regime, although it is difficult to separate the effects of heating rate and of temperature.

Whether or not fading can be observed depends on whether the populations in the steady-state cluster size distribution are higher or lower at higher temperature. That can be ascertained rather simply by considering the equilibrium population at the critical size $N_{n^*}^{eq}$; as can be seen in Fig. 4a, this has its maximum value at the cluster size where all the distributions intersect. The cluster populations (Eq. (3)) depend on $W(n^*)/k_BT$, and values of this parameter, normalized to its minimum value, are plotted in Fig. 5. The different behaviors depend on the temperature dependences of

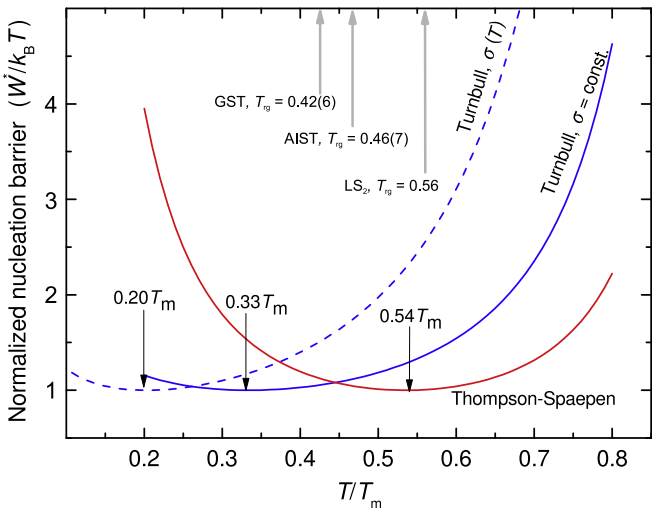

Fig. 5. The nucleation barrier W^*/k_BT, i.e. the argument of the exponential in Eq. (3) for the special case of the critical nucleus, normalized with respect to its minimum value. The barrier shows a minimum as a function of temperature: for temperatures below the minimum the dominant term is T, for temperatures above the minimum the dominant term is W^* which diverges towards infinity as the melting temperature T_m is approached. The simplest case is that for which the thermodynamic driving force for crystallization $\Delta\mu$ is linear with supercooling ΔT (the Turnbull approximation: $\Delta\mu = \Delta H_m \Delta T/T_m N_A$) and the crystal-liquid interfacial energy σ is a temperature-independent constant. For LS_2 the Turnbull approximation is followed closely, but σ shows a slight dependence on temperature (Table 1). For GST and AIST, $\Delta\mu$ is obtained using the Thompson-Spaepen expression Eq. (7), and σ is taken to be constant. In the physically accessible range above the glass-transition temperature, LS_2 shows the barrier only increasing with temperature, while GST and AIST show a narrow temperature range in which the barrier decreases with increasing temperature. (For interpretation of the references to colour in this figure legend, the reader is referred to the web version of this article.)

$\Delta\mu$ and σ. The simplest case is one in which σ is constant (i.e. independent of temperature) and $|\Delta\mu| \propto \Delta T$; it is readily shown analytically that in this case $W(n^*)/k_BT$ is minimum at $0.33T_m$. While this is close to the case of LS_2, the full fitting of nucleation kinetics [23] suggested that σ increases slightly with temperature (Table 1); this gives a minimum at $0.20T_m$. Since for LS_2 $T_{rg} = 0.56$, in the experimentally accessible regime above the glass-transition temperature $W(n^*)/k_BT$ clearly only increases with temperature. Thus, as shown in the particular example in Fig. 2a, a lower temperature would lead to a higher steady-state cluster population.

For GST, our fitting is based on a constant σ and on $\Delta\mu$ following Eq. (7); in that case the minimum in $W(n^*)/k_BT$ is at $0.54T_m$. For GST $T_{rg} = 0.43$, and there is thus a window T_r =0.43–0.54 in which a lower temperature would lead to a lower steady-state cluster population (i.e. fading is possible). We have not attempted a full fitting of nucleation parameters for AIST, but as noted in Section 6, its thermodynamics is similar to that of GST. For AIST the corresponding window in which fading is possible is T_r =0.47–0.54.

5. Priming and fading in GST

We now examine whether the key temperatures identified in our CNT-based treatment of kinetics in GST match those in physical experiments and in atomistic simulations. MD studies of structural changes in GST show that the formation of incipient crystal-like order is fastest at 500 K (specifically faster than at 400 K or 700 K) [18]. It was suggested that this fast ordering may coincide with the temperature at which the steady-state crystal nucleation rate is maximum. The CNT description of kinetics in GST (Fig. 3) shows that the steady-state nucleation rate at 500 K is indeed higher than at 400 K or 700 K. The maximum in the calculated nucleation rate is at ~530 K.

As noted above, Fig. 4b shows that there is a temperature range (383–490 K), just above T_g, in which the effects of a priming treatment might fade with time after the end of the treatment. We now examine how this temperature range relates to studies of priming and fading. The constant low voltage inducing 'pre-structural ordering' in the work of Loke et al. is associated with a temperature rise of ~100 K, and in their MD simulations of this treatment, they take a temperature of 420 K [19]. The fading phenomenon, upon which we focus, was detected after the more intense priming pulses applied by Lee et al. [18]. No estimates are given of the temperature during these priming pulses. This can, however, be estimated from the effects of different priming times. About 50% of the full priming effect is achieved for a single pulse of duration ~60 ns. This characteristic time for changing the cluster size distribution must be similar to the nucleation time-lag θ_{n^*}. From Fig. 3, $\theta_{n^*} = 60$ ns at ~470 K, and we take that as a good estimate of the priming temperature. This temperature is such that on cooling at the end of the treatment, the temperature would be exactly in the range where, according to the cluster size distributions in Fig. 4b, fading would be expected.

From the work of Lee et al. [18], it is clear that the characteristic time of fading is ~1 μs The initial cooling rate at the end of a priming pulse must be very high, and the time to cool to T_g (below which no further evolution of the cluster size distribution is expected) must be much less than 1 μs, perhaps 10–100 ps. Thus the fading time seems unlikely to be determined only by changes in the cluster size distribution during cooling. There may, for example, be effects of a raised base temperature. Given typical thermal diffusivities [4], a time of 1 μs would be associated with a thermal diffusion length of the order of 0.5 μm, comparable with the larger memory cells tested by Lee et al. [18]. We note, consistent with the rapid cooling through the critical temperature range, that even the full extent of

fading ($\Delta t > 1$ μs) is far from removing all the effects of priming.

6. Overall transformation kinetics and device operation

It is important to consider the crystal nucleation kinetics in GST in the context of device operation. Ciocchini et al. have studied crystallization in a phase-change memory (PCM) cell based on a 60 nm GST layer [66]. The transforming volume in this layer has the shape of a mushroom cap. Isothermal crystallization times t_x were measured over an exceptionally wide temperature range, from ~440 K (some 60 K above T_g) right up to the melting point. For the lower temperatures in this range, thermal annealing was used. For the higher temperatures, electrical pulse heating was used, with the temperatures derived from electrical and thermal modeling. Crystallization was detected through change in resistance, with a value of 50 kΩ being used to define t_x for this particular type of PCM cell [66]; in this way t_x corresponds roughly to 50% transformation. The measured crystallization times are plotted in a time-temperature-transformation (TTT) diagram in Fig. 6. Assuming that the SET operation does not require crystal nucleation, but involves only growth, $t_x(T)$ is expected to be minimum at the maximum in growth rate, already noted to be at ~$0.76T_m$ [7]. Above this point, $t_x(T)$ should diverge towards infinity as the temperature is raised to T_m; this feature is not seen in the data, presumably because the temperature in the cell is overestimated. Nonetheless, the values of t_x are interesting. The minimum measured value of ~100 ns is somewhat longer than the time (~30 ns) estimated if a crystal growth front advances at the maximum estimated velocity (~1 m s^{-1} [7]) from one side of the 60 nm GST layer to transform half of the volume.

Fig. 6 also shows the present calculations (Section 3) of the temperature-dependent time-lag $\theta_{n^*}(T)$, in GST. At its minimum, the time-lag is just less than 0.1% of the minimum measured t_x. This shows that crystal nucleation would easily be fast enough to generate growth centers within a PCM cell volume, thereby reducing the growth distances, and switching time, required for the SET operation. In other words, priming is viable for GST. This can also be considered in terms of cooling rates in the RESET operation. The inset in Fig. 6 shows continuous-cooling-transformation (CCT) curves calculated from the TTT curves, assuming *isokinetic* reactions [67]. From the $t_x(T)$ data, the critical cooling rate for glass formation in the PCM cell is ~6×10^8 K s^{-1}. From the $\theta_{n^*}(T)$ data, the critical cooling rate to avoid the formation of subcritical crystalline clusters is ~2×10^{12} K s^{-1}. These values can be estimated roughly from cooling curves in the TTT diagram (dashed black lines in the main part of Fig. 6).

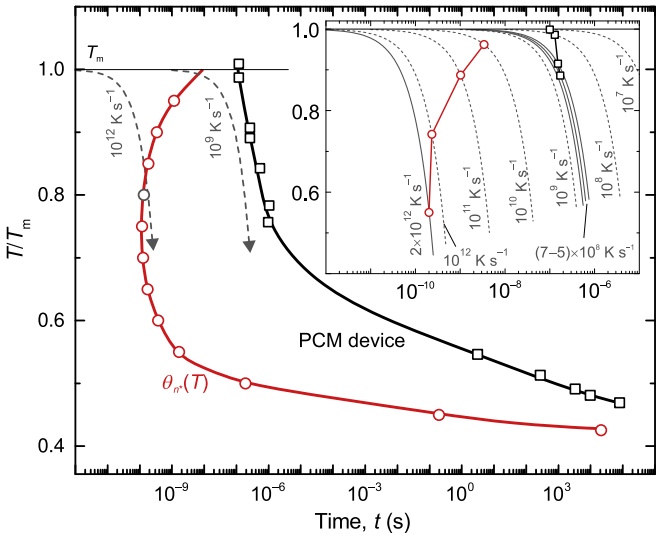

Fig. 6. A time-temperature-transformation (TTT) diagram for the crystallization of GST. The nucleation time-lag $\theta_{n^*}(T)$ is calculated from the parameters derived in the present work (Section 3). The PCM device data are for the SET operation of a cell based on a 60 nm GST layer [66], and show isothermal crystallization times (defined by the resistance of the memory cell decreasing to 50 kΩ). The inset shows the corresponding continuous-cooling-transformation (CCT) diagram, indicating critical cooling rates of ~2×10^{12} K s^{-1} and ~6×10^8 K s^{-1} respectively. The main figure shows traces for constant cooling rate from T_m. (For interpretation of the references to colour in this figure legend, the reader is referred to the web version of this article.)

7. Crystal nucleation in AIST

Based on findings in optical-storage media, the chalcogenides GST and AIST are the archetypes of two classes of crystallization behavior: respectively *nucleation-dominated* and *growth-dominated* [68]. The two systems are thermodynamically rather similar (Table 1), and the distinction between them seems to be mainly kinetic. Recent work [9,11] suggests that this distinction can be considered in terms of the temperature dependence of the viscosity of the liquid. Bulk liquid GST has, throughout its temperature range, a high fragility ($m = 90$). In contrast, AIST appears to show a fragile-to-strong crossover on cooling, from $m = 74$ just above T_m to $m = 37$ just above T_g [11]. (The existence of a crossover has also been suggested in nanoparticles of GST [69]).

In the use of AIST as an optical-storage medium, the equivalent of priming has been demonstrated using laser pulses [26,70]. In the absence of data on nucleation time-lag and on any nucleation rates, however, it is not possible to fit the parameters in CNT as has been done for GST in Fig. 3. Nevertheless it is of interest to consider crystal nucleation kinetics in AIST. We have taken the $\eta(T)$ already derived [9] and calculated $\gamma(T)$ from this using the Stokes–Einstein relation. We have modeled the thermodynamics with the data in Table 1, and used Eq. (7) to estimate the driving force for crystallization. Finally, we have assumed a value of $\sigma = 0.11$ J m^{-2}, estimated using Eq. (8) setting $T = T_g$. The crystalline cluster size distributions at different reduced temperatures are similar to those for GST shown in Fig. 4b and show a somewhat narrower range in which the equilibrium cluster populations are lower at lower temperature.

The corresponding steady-state nucleation rate I^{st} and nucleation time-lag θ_{n^*} for AIST are shown in Fig. 7, compared with the preferred values for GST from Fig. 3. The fragile-to-strong crossover in AIST dramatically suppresses mobility as T_g is approached on cooling. The maximum value of I^{st} in AIST is some sixteen orders of magnitude lower than in GST, and the time-lag in the regime of priming with possible fading is 6–8 orders of magnitude longer. We conclude that while priming of the SET operation in AIST may be possible, it is (with such slow kinetics) very unlikely to be useful in reducing the switching times or the energy consumed.

8. Conclusions

Classical nucleation theory (CNT) has been applied to crystallization of the amorphous chalcogenide GST ($Ge_2Sb_2Te_5$); this crystallization is of interest, for example, as the rate-limiting step in the switching of phase-change random-access memory (PC-RAM). Based on an earlier fitting of the kinetics of crystal growth, a first consistent fitting has been achieved over the entire temperature

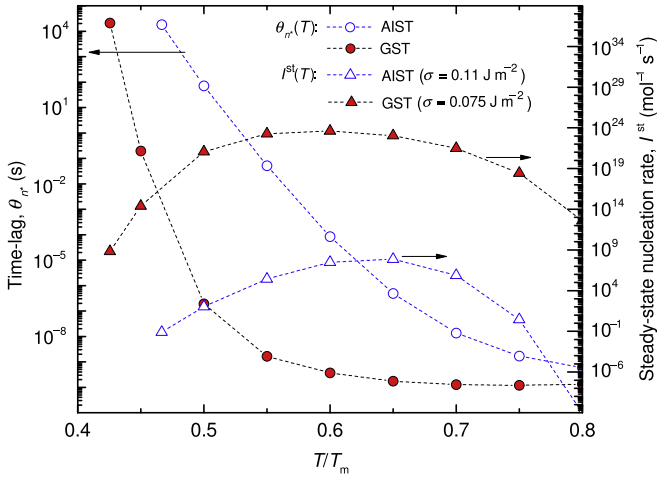

Fig. 7. Comparison of congruent crystallization in supercooled liquid AIST and GST: (a) the nucleation time-lag θ_{n^*}, and (b) the steady-state homogeneous nucleation rate I^{st}, as a function of the homologous temperature. The data for GST correspond to those in Fig. 3. (For interpretation of the references to colour in this figure legend, the reader is referred to the web version of this article.)

range of the supercooled liquid, using values of homogeneous nucleation rate and time-lag obtained from physical experiments and from atomistic simulations. The molecular mobility scales inversely with viscosity according to the Stokes–Einstein relation, and the fitted value of the temperature-independent crystal-liquid interfacial energy is 0.075 J m^{-2}. Consistent with the very high fragility of GST liquid, a match is obtained to the variation of the time-lag over nearly 14 orders of magnitude.

The homogeneous nucleation rate is maximum at a temperature ($0.59T_m$) significantly less than that for the maximum in growth rate ($0.76T_m$). The temperatures of these maxima correspond to the optimum conditions for priming and for the SET operation in PC-RAM. The separate optimum conditions for nucleation and for growth explain how it is possible for priming to reduce the total time and total energy required for crystallization in PC-RAM.

In GST, priming occurs in a temperature range above the glass transition in which the CNT fitting shows that the populations of subcritical crystalline clusters are lower at lower temperature. Thus at the end of a priming pulse when mobility remains high but the temperature falls, the cluster populations briefly fall with time. This accounts for the previously unexplained fading of the effect of priming if there is a time interval between priming and the SET operation, and is a regime of nucleation behavior not present for oxide glass-forming systems such as LS_2 (lithium disilicate).

A similar CNT-based fitting is suggested for the chalcogenide AIST. This shows that priming would be achieved at a homologous temperature of $0.55T_m$, with a nucleation rate ~18 orders of magnitude lower than in GST (at $0.59T_m$), and with a time-lag up to 8 orders longer. Thus priming of AIST is unlikely to be useful in PC-RAM operation. The present analyses reinforce the distinction between the GST and AIST media as, respectively, *nucleation-dominated* and *growth-dominated*.

It had previously been shown that the kinetic aspects of CNT could provide a quantitative basis for predicting the effects of multi-stage anneals in systems such as LS_2. Although the kinetic parameters for GST are very different from those of LS_2, CNT appears to be similarly valid for GST, and complements qualitative characterization of cluster populations by fluctuation transmission electron microscopy. CNT-based modeling gives phase-change timescales that are fully consistent with the operation of actual PCM cells. In future work, full numerical modeling of the evolution of the size distribution of subcritical crystalline clusters may be useful in guiding materials selection and device operation in applications such as PC-RAM.

Acknowledgements

We acknowledge financial support by the World Premier International Research Center Initiative (WPI), MEXT, Japan, and from the European Research Council under the European Union's Horizon 2020 research and innovation program (grant ERC-2015-AdG-695487: ExtendGlass).

References

[1] M. Wuttig, N. Yamada, Phase-change materials for rewritable data storage, Nat. Mater. 6 (2007) 824–832.
[2] P. Hosseini, C.D. Wright, An optoelectronic framework enabled by low-dimensional phase-change films, Nature 511 (2014) 206–211.
[3] D. Kuzum, S. Yu, H.-S.P. Wong, Synaptic electronics: materials, devices and applications, Nanotechnology 24 (2013) 382001.
[4] J.A. Kalb, F. Spaepen, M. Wuttig, Kinetics of crystal nucleation in undercooled droplets of Sb- and Te-based alloys used for phase change recording, J. Appl. Phys. 98 (2005) 054910.
[5] S. Menzel, U. Böttger, M. Wimmer, M. Salinga, Physics of the switching kinetics in resistive memories, Adv. Funct. Mater. 25 (2015) 6306–6325.
[6] H. Neumann, F. Herwig, W. Hoyer, The short range order of liquid eutectic A_{III}-Te and A_{IV}-Te alloys, J. Non-Cryst. Solids 205–207 (1996) 438–442.
[7] J. Orava, A.L. Greer, B. Gholipour, D.W. Hewak, C.E. Smith, Characterization of supercooled liquid $Ge_2Sb_2Te_5$ and its crystallization by ultrafast-heating calorimetry, Nat. Mater. 11 (2012) 279–283.
[8] G.C. Sosso, J. Behler, M. Bernasconi, Breakdown of Stokes-Einstein relation in the supercooled liquid state of phase change materials, Phys. Status Solidi. B 249 (2012) 1880–1885.
[9] J. Orava, D.W. Hewak, A.L. Greer, Fragile-to-strong crossover in supercooled liquid Ag-In-Sb-Te studied by ultrafast calorimetry, Adv. Funct. Mater. 25 (2015) 4851–4858.
[10] S. Wei, P. Lucas, C.A. Angell, Phase change alloy viscosities down to T_g using Adam-Gibbs-equation fittings to excess entropy data: a fragile-to-strong transition, J. Appl. Phys. 118 (2015) 034903.
[11] J. Orava, H. Weber, I. Kaban, A.L. Greer, Viscosity of liquid Ag-In-Sb-Te: evidence of a fragile-to-strong crossover, J. Chem. Phys. 144 (2016) 194503.
[12] T. Ishikawa, P.-F. Paradis, J.T. Okada, Y. Watanabe, Viscosity measurements of molten refractory metals using an electrostatic levitator, Meas. Sci. Technol. 23 (2012) 025305.
[13] V. Weidenhof, I. Friedrich, S. Ziegler, M. Wuttig, Laser induced crystallization of amorphous $Ge_2Sb_2Te_5$ films, J. Appl. Phys. 89 (2001) 3168–3176.
[14] J. Wei, F. Gan, Theoretical explanation of different crystallization processes between as-deposited and melt-quenched amorphous $Ge_2Sb_2Te_5$ thin films, Thin Solid Films 441 (2003) 292–297.
[15] D. Hewak, B. Gholipour, Primed to remember, Science 336 (2012) 1515–1516.
[16] K. Johguchi, T. Shintani, T. Morikawa, K. Yoshioka, K. Takeuchi, ×10 Fast write, 80% energy saving temperature controlling set method for multi-level cell phase change memories to solve the scaling blockade, Solid State Electron. 81 (2013) 78–85.
[17] D. Loke, J.M. Skelton, W.-J. Wang, T.-H. Lee, R. Zhao, T.-C. Chong, S.R. Elliott, Ultrafast phase-change logic device driven by melting processes, Proc. Nat. Acad. Sci. 111 (2014) 13272–13277.
[18] T.H. Lee, D. Loke, K.-J. Huang, W.-J. Wang, S.R. Elliott, Tailoring transient-amorphous States: towards fast and power-efficient phase-change memory and neuromorphic computing, Adv. Mater. 26 (2014) 7493–7498.
[19] D. Loke, T.H. Lee, W.J. Wang, L.P. Shi, R. Zhao, Y.C. Yeo, T.C. Chong, S.R. Elliott, Breaking the speed limits of phase-change memory, Science 336 (2012) 1566–1569.
[20] K.F. Kelton, A.L. Greer, C.V. Thompson, Transient nucleation in condensed systems, J. Chem. Phys. 79 (1983) 6261–6276.
[21] K.F. Kelton, A.L. Greer, Transient nucleation effects in glass formation, J. NonCryst. Solids 79 (1986) 295–309.
[22] K.F. Kelton, A.L. Greer, Test of classical nucleation theory in a condensed system, Phys. Rev. B 38 (1988) 10089–10092.
[23] A.L. Greer, K.F. Kelton, Nucleation in lithium disilicate glass: a test of classical theory by quantitative modeling, J. Am. Ceram. Soc. 74 (1991) 1015–1022.
[24] S. Senkader, C.D. Wright, Models for phase-change of $Ge_2Sb_2Te_5$ in optical and electrical memory devices, J. Appl. Phys. 95 (2004) 504–511.
[25] K. Darmawikarta, B.-S. Lee, R.M. Shelby, S. Raoux, S.G. Bishop, J.R. Abelson, Quasi-equilibrium size distribution of subcritical nuclei in amorphous phase change AgIn-Sb_2Te, J. Appl. Phys. 114 (2013) 034904.
[26] B.-S. Lee, G.W. Burr, R.M. Shelby, S. Raoux, C.T. Rettner, S.N. Bogle, K. Darmawikarta, S.G. Bishop, J.R. Abelson, Observation of the role of subcritical nuclei in crystallization of a glassy solid, Science 326 (2009) 980–984.

[27] B.-S. Lee, R.M. Shelby, S. Raoux, C.T. Retter, G.W. Burr, S.N. Bogle, K. Darmawikarta, S.G. Bishop, J.R. Abelson, Nanoscale nuclei in phase change materials: origin of different crystallization mechanisms of $Ge_2Sb_2Te_5$ and AgInSbTe, J. Appl. Phys. 115 (2014) 063506.
[28] B.-S. Lee, K. Darmawikarta, S. Raoux, Y.-H. Shih, Y. Zhu, S.G. Bishop, J.R. Abelson, Distribution of nanoscale nuclei in the amorphous dome of a phase change random access memory, Appl. Phys. Lett. 104 (2014) 071907.
[29] K. Darmawikarta, S. Raoux, P. Tchoulfian, T. Li, J.R. Abelson, S.G. Bishop, Evolution of subcritical nuclei in nitrogen-alloyed $Ge_2Sb_2Te_5$, J. Appl. Phys. 112 (2012) 124907.
[30] G.W. Burr, P. Tchoulfian, T. Topuria, C. Nyffeler, K. Virwani, A. Padilla, R.M. Shelby, M. Eskandari, B. Jackson, B.-S. Lee, Observation and modeling of polycrystalline grain formation in $Ge_2Sb_2Te_5$, J. Appl. Phys. 111 (2012) 104308.
[31] J. Akola, R.O. Jones, Structural phase transitions on the nanoscale: the crucial pattern in the phase-change materials $Ge_2Sb_2Te_5$ and GeTe, Phys. Rev. B 76 (2007) 235201.
[32] J. Hegedüs, S.R. Elliott, Microscopic origin of the fast crystallization ability of Ge-Sb-Te phase-change memory materials, Nat. Mater. 7 (2008) 399–405.
[33] J. Akola, R.O. Jones, Structure of liquid phase change material AgInSbTe from density functional/molecular dynamics simulations, Appl. Phys. Lett. 94 (2009) 251905.
[34] J.M. Skelton, D. Loke, T.H. Lee, S.R. Elliott, Understanding the multistate SET process in Ge-Sb-Te-based phase-change memory, J. Appl. Phys. 112 (2012) 064901.
[35] J.M. Skelton, D. Loke, T.H. Lee, S.R. Elliott, Structural insights into the formation and evolution of amorphous phase-change materials, Phys. Status Solidi. B 250 (2013) 968–975.
[36] P. Noé, C. Sabbione, N. Bernier, N. Castellani, F. Fillot, F. Hippert, Impact of interfaces on scenario of crystallization of phase change materials, Acta Mater. 110 (2016) 142–148.
[37] N. Ciocchini, D. Ielmini, Pulse-induced crystallization in phase-change memories under set and disturb conditions, IEEE Trans. Electron. Dev. 62 (2015) 847–854.
[38] V.G. Karpov, Y.A. Kryukov, S.D. Savransky, I.V. Karpov, Nucleation switching in phase change memory, Appl. Phys. Lett. 90 (2007) 123504.
[39] K.F. Kelton, Crystal nucleation in liquids and glasses, in: H. Ehrenreich, D. Turnbull (Eds.), Solid State Physics, Academic Press, Boston, MA, 1991, pp. 75–178.
[40] K.F. Kelton, A.L. Greer, Nucleation in Condensed Matter, Applications in Materials and Biology, Elsevier, Oxford, 2010.
[41] M.D. Ediger, P. Harrowell, L. Yu, Crystal growth kinetics exhibit a fragility-dependent decoupling from viscosity, J. Chem. Phys. 128 (2008) 034709.
[42] J.W.P. Schmelzer, A.S. Abyzov, V.G. Baidakov, Time of formation of the first supercritical nucleus, time-lag, and the steady-state nucleation rate, Appl. Glass Sci. 8 (2017) 48–60.
[43] C.A. Angell, Formation of glasses from liquids and biopolymers, Science 267 (1995) 1924–1935.
[44] J. Orava, A.L. Greer, Fast and slow crystal growth kinetics in glass-forming melts, J. Chem. Phys. 140 (2014) 214504.
[45] R. Jeyasingh, S. Fong, J. Lee, Z. Li, K.-W. Chang, D. Mantegazza, M. Asheghi, K.E. Goodson, H.-S.P. Wong, Ultra-fast characterization of phase-change material crystallization properties in the melt-quenched amorphous phase, Nano Lett. 14 (2014) 3419–3426.
[46] A. Sebastian, M. Le Gallo, D. Krebs, Crystal growth within a phase change memory cell, Nat. Commun. 5 (2014) 4314.
[47] J. Orava, A.L. Greer, Fast crystal growth in glass-forming liquids, J. Non Cryst. Solids 451 (2016) 94–100.
[48] J. Orava, A.L. Greer, B. Gholipour, D.W. Hewak, C.E. Smith, Ultra-fast calorimetry study of $Ge_2Sb_2Te_5$ crystallization between dielectric layers, Appl. Phys. Lett. 101 (2012) 091906.
[49] C.V. Thompson, F. Spaepen, On the approximation of the free energy change on crystallization, Acta Metall. 27 (1979) 1855–1859.
[50] L. Battezzati, A.L. Greer, Thermodynamics of $Te_{80}Ge_{20-x}Pb_x$ glass-forming alloys, J. Mater. Res. 3 (1988) 570–575.
[51] V.M. Fokin, E.D. Zanotto, Crystal nucleation in silicate glasses: the temperature and size dependence of crystal/liquid surface energy, J. Non Cryst. Solids 265 (2000) 105–112.
[52] F. Spaepen, R.B. Meyer, The surface tension in a structural model for the solid-liquid interface, Scr. Metall. 10 (1976) 257–263.
[53] K. Matusita, M. Tashiro, Rate of homogeneous nucleation in alkali disilicate glasses, J. Non-Cryst. Solids 11 (1973) 471–484.
[54] J. Kalb, F. Spaepen, M. Wuttig, Calorimetric measurements of phase transformations in thin films of amorphous Te alloys used for optical data storage, J. Appl. Phys. 93 (2003) 2389–2393.
[55] T.H. Lee, S.R. Elliott, Ab initio computer simulation of the early stages of crystallization: application to $Ge_2Sb_2Te_5$ phase-change materials, Phys. Rev. Lett. 107 (2011) 145702.
[56] T.H. Lee, D. Loke, S.R. Elliott, Microscopic mechanism of doping-induced kinetically constrained crystallization in phase-change materials, Adv. Mater. 17 (2015) 5477–5483.
[57] G. Ruitenberg, A.K. Petford-Long, R.C. Doole, Determination of the isothermal nucleation and growth parameters for the crystallization of thin $Ge_2Sb_2Te_5$ films, J. Appl. Phys. 92 (2002) 3116–3123.
[58] X. Wei, L. Shi, T.C. Chong, R. Zhao, H.K. Lee, Thickness dependent nanocrystallization in $Ge_2Sb_2Te_5$ films and its effect on devices, Jpn. J. Appl. Phys. 46 (2007) 2211–2214.
[59] S. Privitera, C. Bongiorno, E. Rimini, R. Zonca, Crystal nucleation and growth processes in $Ge_2Sb_2Te_5$, Appl. Phys. Lett. 84 (2004) 4448–4450.
[60] S. Privitera, S. Lombardo, C. Bongiorno, E. Rimini, A. Pirovano, Phase change mechanisms in $Ge_2Sb_2Te_5$, J. Appl. Phys. 102 (2007) 013516.
[61] J. Kalb, F. Spaepen, M. Wuttig, Atomic force microscopy measurements of crystal nucleation and growth rates in thin films of amorphous Te alloys, Appl. Phys. Lett. 84 (2004) 5240–5242.
[62] U. Russo, D. Ielmini, A.L. Lacaita, Analytical modeling of chalcogenide crystallization for PCM data-retention extrapolation, IEEE Trans. Electron. Dev. 54 (2007) 2769–2777.
[63] T. Gille, K. De Meyer, D.J. Wouters, Amorphous-crystalline phase transitions in chalcogenide materials for memory applications, Phase Transit. 81 (2008) 773–790.
[64] K. Kohary, C.D. Wright, Modelling the phase-transition in phase-change materials, Phys. Status Solidi. B 250 (2013) 944–948.
[65] S. Kozyukhin, T. Vorobyov, A. Sherchenkov, A. Babich, N. Vishnyakov, O. Boytsova, Isothermal crystallization of $Ge_2Sb_2Te_5$ amorphous thin films and estimation of information reliability of PCM cells, Phys. Status Solidi A 213 (2016) 1831–1838.
[66] N. Ciocchini, M. Cassinerio, D. Fugazza, D. Ielmini, Evidence for non-Arrhenius kinetics of crystallization in phase change memory devices, IEEE Trans. Electron. Dev. 60 (2013) 3767–3774.
[67] J.W. Cahn, Transformation kinetics during continuous cooling, Acta Metall. 4 (1956) 572–575.
[68] G.-F. Zhou, Materials aspects in phase change optical recording, Mater. Sci. Eng. A 304–306 (2001) 73–80.
[69] B. Chen, G.H. ten Brink, G. Palasantzas, B.J. Kooi, Crystallization kinetics of GeSbTe phase-change nanoparticles resolved by ultrafast calorimetry, J. Phys. Chem. C 121 (2017) 8569–8579.
[70] Y. Wang, F.Y. Zuo, H. Huang, F.X. Zhai, T.S. Lai, Y.Q. Wu, Transient phase change in picosecond laser pulse-driven crystallization process, Proc. SPIE 7517 (2009) 75170S.